

Confinement and lack of thermalization after quenches in the bosonic Schwinger model

Titas Chanda,^{1,*} Jakub Zakrzewski,^{1,2} Maciej Lewenstein,^{3,4} and Luca Tagliacozzo^{5,6}

¹*Instytut Fizyki im. Marii Smoluchowskiego, Uniwersytet Jagielloński, Lojasiewicza 11, 30-348 Kraków, Poland*

²*Mark Kac Complex Systems Research Center, Uniwersytet Jagielloński, Kraków, Poland*

³*ICFO-Institut de Ciències Fotòniques, The Barcelona Institute of Science and Technology, Av. Carl Friedrich Gauss 3, 08860 Castelldefels (Barcelona), Spain*

⁴*ICREA, Passeig Lluís Companys 23, 08010 Barcelona, Spain*

⁵*Department of Physics and SUPA, University of Strathclyde, Glasgow G4 0NG, UK*

⁶*Departament de Física Quàntica i Astrofísica and Institut de Ciències del Cosmos (ICCUB), Universitat de Barcelona, Martí i Franquès 1, 08028 Barcelona, Catalonia, Spain*

We excite the vacuum of a relativistic theory of bosons coupled to a $U(1)$ gauge field in $1+1$ dimensions (bosonic Schwinger model) out of equilibrium by creating a spatially separated particle-antiparticle pair connected by a string of electric field. During the evolution, we observe a strong confinement of the bosons witnessed by the bending of their light cone, reminiscent of what has been observed for the Ising model [Nat. Phys. **13**, 246 (2017)]. As a consequence, for the time scales we are able to simulate, the system evades thermalization and generates exotic asymptotic states. These states are made of two disjoint regions, an external deconfined region that seems to thermalize, and an inner core that reveals an area-law saturation of the entanglement entropy.

Introduction.— Solving the out-of-equilibrium dynamics (OED) of large many-body quantum systems becomes exponentially hard when the number of constituents increases beyond few tens. This fact hinders our understanding of important questions such as the existence of new phases of matter [1–3] and the presence or absence of thermalization [4–7].

Symmetries play a crucial role out of equilibrium as they give rise to conservation laws and continuity equations that can strongly constrain the dynamics [8–10]. Local symmetries can also have strong consequences in the OED since they are responsible for interesting phenomena, such as slow dynamics and localization [11–16].

The simplest system with local symmetries is the fermionic Schwinger model (FSM) [17], the quantum electrodynamics in $1+1$ dimensions (1D). The FSM, by now, has been studied extensively with traditional methods [11, 18–23] and with tensor-network techniques [24–32]. In 1D, the gauge field does not describe dynamical photons but rather gives rise to long-range interactions among the matter fields. However, the FSM share common features with quantum chromodynamics (QCD) (confinement, a non-trivial vacuum exhibiting chiral symmetry breaking etc.).

Here we consider the OED of the bosonic version of the Schwinger model [17–19] (BSM), i.e., the 1D scalar quantum electrodynamics, consisting of bosonic matter coupled to an $U(1)$ gauge field. Surprisingly, the BSM is much less studied than the FSM even though it has recently been shown that considering the bosonic version of well studied fermionic models can unveil unexpected new phenomena [33–35]. Moreover, the quantum simulation of bosons coupled to gauge fields is also easier to realize in experiments with ultra-cold atoms [36–39], something very relevant at a stage when the quantum simulation of dynamical gauge fields is a reality [40–46].

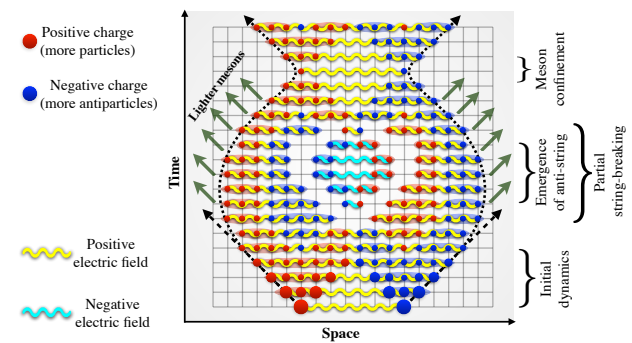


FIG. 1. (Color online.) Semi-classical sketch of the confining dynamics of BSM. We prepare a well separated pair of particle and antiparticle connected by an electric-flux tube. Initially they start spreading as if they were free, however their trajectories bend due to the energetic cost of creating larger electric-flux tubes. New dynamical charges are also created during the evolution and partially screen the electric field. Still the electric field oscillates coherently and can form an anti-string, creating a central core of strongly correlated bosons. The density of bosons in the core can get depleted through the radiation of lighter mesons that freely propagate.

The Hamiltonian version of the BSM is made by two bosonic species that behave, in the non-interacting regime, as a discretized version of Lorentz-invariant free bosonic theory, the Klein-Gordon (KG) field theory [47–50]. One species represents the particle of the KG theory and the other the anti-particle, where both are coupled to a $U(1)$ gauge field. The low energy spectrum of this system is always gapped, as in the FSM and QCD, even for massless bosons [50]. By using state-of-the-art matrix-product states (MPS) techniques [51–63] in their gauge-invariant version [24, 25, 64–69], we analyze the OED in both the massless and the massive regimes of the theory.

At any value of the bare mass, bosons are tightly confined, much more than fermions. This is observed, for example, by creating a particle-antiparticle pair separated by a given distance and letting them evolve. Fig. 1 contains a cartoon sketch of the dynamics, where two bosons are connected by an electric-flux tube that bends trajectories of the bosons inwards. Such dynamics is different from the one observed in the fermionic case [30, 68], and bears a strong similarity to observations for Ising model [70]. Similar results have been obtained in the context of holographic quenches [71–75], spins systems [11–13], large N gauge theories [16] and quantum link models [14]. Here we observe it for the first time in a bosonic lattice gauge theory and we attribute it to the partial screening of the electric field by the dynamically generated particles.

The initial bosons form a core of strongly correlated matter that oscillates several times around its original position. In the small mass regime, the matter density in the core is gradually depleted by the radiation of free lighter mesons. Even after the bosons have left the region, the core stays quantitatively different from the rest of the system (as shown, for e.g., by the entanglement entropy). We believe this phenomenon is a form of slow dynamics that prevents thermalization, such as the one observed in [76, 77]. We characterize this feature in terms of entropy production [4, 78].

Model.— The BSM Lagrangian density is given by $\mathcal{L} = -[D_\mu \phi]^* D^\mu \phi - m^2 |\phi|^2 - \frac{1}{4} F_{\mu\nu} F^{\mu\nu}$ [79], where ϕ is the complex scalar field, $D_\mu = (\partial_\mu + iqA_\mu)$ is the covariant derivative with q and A_μ being the electronic-charge and vector potential respectively, m is the bare mass of the particles, and $F_{\mu\nu}$ is the electromagnetic field tensor. In 1D, after fixing the temporal gauge, $A_t = 0$, we get the discretized Hamiltonian (in dimensionless units) as [50, 80]

$$\hat{H} = \sum_j \hat{L}_j^2 + 2(x((m/q)^2 + 2x))^{1/2} \sum_j (\hat{a}_j^\dagger \hat{a}_j + \hat{b}_j^\dagger \hat{b}_j^\dagger) - \frac{x^{3/2}}{((m/q)^2 + 2x)^{1/2}} \sum_j [(\hat{a}_{j+1}^\dagger + \hat{b}_{j+1}) \hat{U}_j (\hat{a}_j + \hat{b}_j^\dagger) + \text{h.c.}] \quad (1)$$

where $\{\hat{a}_j^\dagger, \hat{a}_j\}$, $\{\hat{b}_j^\dagger, \hat{b}_j\}$ are the bosonic creation-annihilation operators corresponding to charged particles and antiparticles respectively, \hat{L}_j is the electric field operator residing on the bond between sites j and $j+1$ with $\{\hat{U}_j, \hat{U}_j^\dagger\}$ being $U(1)$ ladder operators satisfying $[\hat{L}_j, \hat{U}_l] = -\hat{U}_j \delta_{jl}$ and $[\hat{L}_j, \hat{U}_l^\dagger] = \hat{U}_j^\dagger \delta_{jl}$, and $x = 1/(a^2 q^2)$ with a being the lattice-spacing.

The Hamiltonian is invariant under local $U(1)$ transformations: $\hat{a}_j \rightarrow e^{i\alpha_j} \hat{a}_j$, $\hat{b}_j \rightarrow e^{-i\alpha_j} \hat{b}_j$, $\hat{U}_j \rightarrow e^{-i\alpha_j} \hat{U}_j e^{i\alpha_{j+1}}$, where the corresponding Gauss law generators are given by $\hat{G}_j = \hat{L}_j - \hat{L}_{j-1} - \hat{Q}_j$, with $\hat{Q}_j = \hat{a}_j^\dagger \hat{a}_j - \hat{b}_j^\dagger \hat{b}_j$ being the dynamical charge [50, 80]. The physical subspace is spanned by the set of states,

$|\Psi\rangle$, that are annihilated by \hat{G}_j , i.e., $\hat{G}_j |\Psi\rangle = 0 \ \forall j$. Using this conservation law, in an open chain, one can integrate-out the gauge fields using the transformation, $\hat{L}_j = \sum_{l \leq j} \hat{Q}_l$, where we consider the static electric field on the left of the chain to be zero. The effective Hamiltonian for matter fields, once we have integrated out the photons, contains long-range intra-species repulsion and inter-species attraction.

The continuum limit of the system is achieved by taking the two limits: $N \rightarrow \infty$ and $x \rightarrow \infty$. However, since our study is motivated by the near future experimental realizations with cold-atoms we consider an open chain made of a finite number of lattice sites $N = 60$ with $N-1 = 59$ bonds, at the experimentally relevant $x = 2$. We obtain systematic matrix-product state approximations to the the ground-state of the system using the density matrix renormalization group (DMRG) [51, 81–83]. This is the starting point for the time-evolution, that we approximate by using the time-dependent variational principle (TDVP) [58, 59, 63, 84, 85] (see [80] for more details).

Real-time evolution.— We start the OED of the BSM by creating two extra dynamical charges of opposite signs on the top of the ground state $|\Omega\rangle$ of the Hamiltonian in Eq. (1). They are located at positions $N/2 - R$ and $N/2 + R + 1$ respectively, and are connected by a string of electric field of length $2R + 1$. They are created by means of the non-local operator \hat{M}_R , defined as

$$\hat{M}_R \equiv \left(\hat{a}_{\frac{N}{2}-R}^\dagger + \hat{b}_{\frac{N}{2}-R}^\dagger \right) \left[\prod_{j=\frac{N}{2}-R}^{\frac{N}{2}+R} \hat{U}_j^\dagger \right] \left(\hat{a}_{\frac{N}{2}+R+1} + \hat{b}_{\frac{N}{2}+R+1}^\dagger \right). \quad (2)$$

As a result, the initial state is $|\psi(t=0)\rangle = \mathcal{N} \hat{M}_R |\Omega\rangle$, where \mathcal{N} is a normalization constant. The state has extra energy $\approx (2R+1) + 4(x((m/q)^2 + 2x))^{1/2}$ above the ground state energy. When R is a finite fraction of the system size, the initial state has an extensive extra energy, thus in principle fulfilling the condition for thermalization. The extra energy is contained in the electric-flux tube joining the two charges, extensive in R . As a result, the evolution of $|\psi(t=0)\rangle$ under (1) is mostly driven by high-energy excited states.

Confinement and string-breaking.— We would expect the charges, initially created at distance $2R+1$, to separate by stretching the electric-flux string up to a critical distance that only depends on the boson mass. There ultimately the string would break as a result of boson pair-production from the vacuum. After that, lighter mesons would propagate freely (similarly to the FSM case [30]). However, in the BSM we do not observe such a scenario. We only see a partial screening of the initial electric-field string, leading to a partial string-breaking, even for massless bosons. Our observations can be explained using a semi-classical cartoon presented in Fig. 1 displaying four main features of the OED:

Partial screening of electric field: Initially, as the two

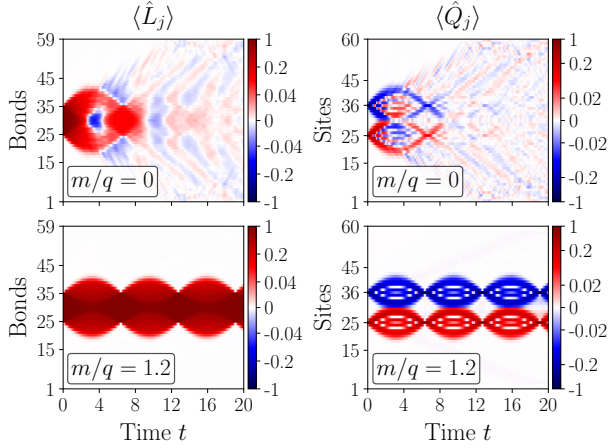


FIG. 2. (Color online.) Dynamics of the electric field \hat{L}_j and the dynamical charge \hat{Q}_j for $R = 5$.

test charges start spreading, they partially screen the electric-field string, so that their light-cone structure gets drastically modified. The charges indeed slow-down their spreading and start to refocus.

String-inversion in the bulk: As observed recently in the dynamics of $U(1)$ quantum link models [14], the string does not break, not even for massless bosons, but rather undergoes at least a pair of coherent oscillations. For lighter masses, we observe a string-inversion phenomenon that renders the dynamics slow. Also for lighter masses, the coherent dynamics of the string is slowly damped by the radiation of lighter mesons.

Mesons radiation, the two domains: While in the bulk the string contracts and expands periodically, at the boundaries the electric flux is partially screened and the string can break into pieces forming lighter mesons. They are free to escape the confined region and fly away with a constant velocity. This effectively creates two separate domains, a core region where the bosons are confined (a confined domain), and an outer region where they escape in the form of light mesons (a deconfined domain). The radiation of light mesons slowly depletes the electric field and the cloud of bosons in the confined region.

Confinement resulting in slow dynamics: We observe that the effects of confinement are much stronger compared to what was observed for FSM. The electric-flux string creates a long-lived metastable state in the middle of the system that oscillates and contract inwards [12, 71, 74, 75], reducing the velocity of charges and bending the initial light cone [70]. The two charges are thus confined again into an extended meson, that wobbles at a well defined frequency (Fig. 1).

The cartoon in Fig. 1 tries to summarize the numerical results presented in Fig. 2. There we plot both the electric field (\hat{L}_j) on the left and the dynamical charges (\hat{Q}_j) on the right for two paradigmatic values $m/q = 0$ and 1.2 that together display all the phenomena we have listed previously. The dynamics is generated by acting the operator $\hat{M}_{R=5}$ (Eq. (2)) on the vacuum of (1). In the massless scenario (top row of Fig. 2), we appreciate the *partial screening* of the electric field, visible in the bending of the bosons' light cone; the appearance of an *anti-string* in the bulk of the system due to the *string-inversion* at $t \simeq 2.5$; the *meson radiation* from the edges of the confined bulk starting around $t \gtrsim 4$. We also see that the confined core of bosons is gradually depleted and disappears for times around $t \simeq 10$.

As we increase the mass, we slowly move towards the heavy-bosons scenario of $m/q = 1.2$ (bottom row of Fig. 2), where the radiation of free mesons is strongly suppressed and the confined core is basically surrounded by the vacuum. We indeed observe an almost perfect periodic oscillation of the electric string. Intermediate regimes (not shown, see [80]) display interesting features. For example for $m/q = 0.25$, the anti-string, visible in $m/q = 0$ case, disappears and there is no string-breaking for $m/q \gtrsim 0.5$.

While for $m/q = 0$ the concentration of dynamical charges in the confined domain gradually disappears for $t \gtrsim 10$, it persists in the asymptotic states for larger values of the mass. However, the confined core still lingers on for a long time, even in the massless case, which can be perceived through the fluctuation of \hat{L}_j or \hat{Q}_j , or through the spreading of the entanglement entropy.

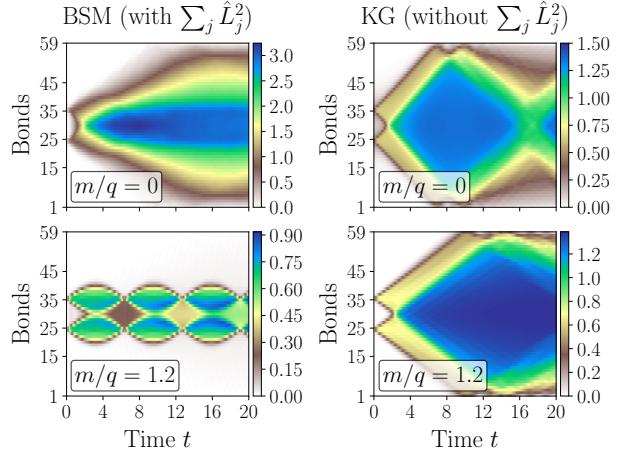


FIG. 3. (Color online.) Dynamics of entanglement in the BSM (left column) and in the non-interacting KG system (right column). We plot the entanglement entropy of the time-evolved state after subtracting the entropy of respective ground state $|\Omega\rangle$ and consider $R = 5$.

Entanglement dynamics.— The best way to characterize the slow dynamics is by considering the growth and spreading of entanglement. The entanglement entropy, \mathcal{S}_j , measured across the bond between the sites j and $j+1$ is defined as $\mathcal{S}_j(t) = -\text{Tr}[\rho_j(t) \ln \rho_j(t)]$, with $\rho_j(t) = \text{Tr}_{j+1,j+2,\dots,N} |\psi(t)\rangle \langle \psi(t)|$ being the reduced density matrix to the left of the j^{th} bond. We study $\mathcal{S}_j(t)$ for all j , and compare it with what is observed in a non-interacting KG system, obtained by dropping $\sum_j \hat{L}_j^2$ term from the Hamiltonian.

Fig. 3 contains $\mathcal{S}_j(t)$ for the interacting BSM (left column), and the the non-interacting KG model (right column) for all bonds j . For the KG model the entanglement spreads linearly with a light-cone structure as predicted by the pseudo-particle picture. For a given $j \ll N/2$, it initially increases ballistically with time and saturates to a value proportional to the volume of the region as predicted by [86] and recently discussed in the context of generalized thermalization [4, 78]. The particles bouncing off the boundaries induce the observed recurrences.

In the BSM, the spread of entanglement is strongly modified by the effects of confinement (left column). Initially its spreading slows-down, and only starts to spread ballistically in correspondence to the radiation of free mesons for lighter masses. Furthermore, most of the entanglement is contained in the region that is initially occupied by the confined bosonic matter, and persists there even long after the concentration of bosons in the bulk has disappeared at around $t \simeq 10$. On the other hand, the concentration of entanglement never leaks into the deconfined domain for heavier bosons, e.g., $m/q = 1.2$. Such unusual dynamics of entanglement clearly indicate a strong reluctance towards thermalization (c.f. [11]) as the presence of memory effect in the dynamics is evident.

Classical and distillable entanglement.— As part of the gauge symmetry, the system possesses a global $U(1)$ symmetry corresponding to the conservation of total dynamical charge, $\sum_j \hat{Q}_j$. As a result any reduced density matrix is block-diagonal in different charge sectors: $\rho = \bigoplus_Q \tilde{\rho}_Q = \bigoplus_Q p_Q \rho_Q$, where $p_Q = \text{Tr}[\tilde{\rho}_Q]$ and $\rho_Q = \tilde{\rho}_Q/p_Q$. Therefore, following [87–94] the entanglement entropy can be divided into two parts as $\mathcal{S}(\rho) = -\sum_Q p_Q \ln p_Q + \sum_Q p_Q \mathcal{S}(\rho_Q)$, where the first term is the classical part (\mathcal{S}^C) – the Shannon entropy between different quantum blocks indicated by $Q \in \{.., -1, 0, 1, ..\}$, and the second term is the distillable entanglement (\mathcal{S}^Q) that can be extracted from the system using *local operations and classical communication* (LOCC).

Fig. 4 shows the time-evolution of both the parts of entanglement entropy, where we observe that the classical part demarcates confined and deconfined domains by remaining *sharply* concentrated only in the confined domain. Since the relevant energy-scales in the dynamics are much larger than the corresponding mass-gaps [50], contributions of different quantum-blocks, other than $Q = 0$, are not negligible in the confined domain. On the

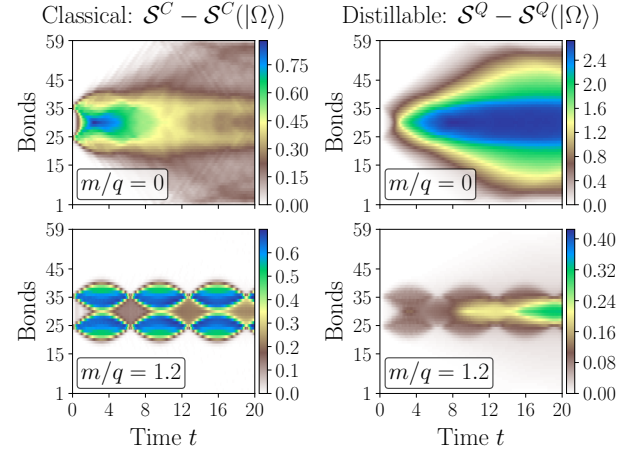


FIG. 4. (Color online.) Time-evolution of the classical part \mathcal{S}^C of entanglement entropy (left column) and the distillable entanglement entropy \mathcal{S}^Q (right column). Here we subtract the corresponding entropies of the ground state $|\Omega\rangle$ and consider the case of $R = 5$.

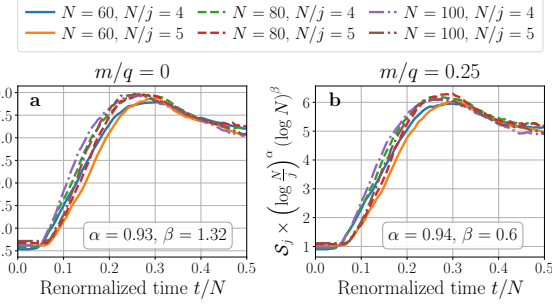


FIG. 5. (Color online.) Pattern of entanglement entropy in the deconfined domain for different system and bipartition sizes.

other hand, free lighter mesons are essentially one particle excitations. Therefore, the only relevant quantum-blocks present in the deconfined domain are $Q = 0, \pm 1$ with $p_{Q=0} \ll p_{Q=\pm 1}$, as these free mesons are made of a very small amount of opposite dynamical charges. That is why \mathcal{S}^C possesses visibly small values outside the confined core. The distillable entanglement entropy, however, shows the same behavior as the total entropy. This seems to suggest that the slow dynamics is not caused by the super-selection sectors induced by the global subgroup of the local symmetry. It is also important to mention here that on average $\mathcal{S}^Q > \mathcal{S}^C$ for smaller masses, where we have both confined and deconfined domains, while for the heavier bosons, e.g., $m/q = 1.2$, the distillable entanglement is less than the classical part.

Lack of thermalization.— From the above discussions it is clear that confinement strongly hinders the thermalization process in the system and the ‘equilibrated’ states

are far from thermal. In the thermal situation, the entropy of a region grows proportional to its size (volume-law), while in the non-ergodic scenario the entropy increases slower than that.

To analyze the scaling of the entropy with the system size in the asymptotic states, we consider $N = 60, 80$, and 100 and $R = N/10$, so that the length of the initial string grows proportional to the system size. In this way we are sure that the initial state has an extensive amount of energy on the top of the ground state, prerequisite for thermalization. We expect that the deconfined domain slowly becomes thermal, due to the radiation of light mesons, while the confined domain remains “non-thermal” showing coherent oscillations. In the confined domain, identified by the position of the initial string, i.e., the bonds $N/2 - R$ to $N/2 + R$, the entropy shows a perfect area-law. Its saturated value does not depend on the size of the region. For long times, the same behavior is seen in the average entropy over the confined domain region, $\mathcal{S}^{Av} = \frac{1}{2R+1} \sum_{j=N/2-R}^{N/2+R} \mathcal{S}_j$ (see [80]). This behavior is a clear indication of the lack of thermalization.

Outside the confined region, the entropy increases with the size of the bipartition. From scaling plots, we find that the entropy varies as $\mathcal{S}_j \propto \left(\log \frac{N}{j}\right)^{-\alpha} (\log N)^{-\beta}$ where the exponents $\alpha \approx 1$ and β depend on m/q (see Fig. 5). For fixed N , the entropy increases sub-linearly for small bipartitions, then turns into a linear increase for intermediate distances, and ultimately shows faster than volume-law growth before saturating into the confined domain. From this scaling form, it seems reasonable to expect that the deconfined region would actually thermalize at intermediate distances, far away from both the core and the boundaries of the system. This complicated scaling form seems to match the behavior expected in a thermalized region with the presence of a physical boundary and of a confined core.

Conclusion.— We have shown that the out-of-equilibrium dynamics generated by creating a pair of bosons on the top of the interacting vacuum of a gauge theory is strongly affected by confinement. The asymptotic states generated are highly inhomogeneous. They are made by a confined core that displays long-lived oscillations and entropically fulfills the area-law, surrounded either by the vacuum (for heavy bosons) or by an almost thermal cloud of light mesons (for lighter bosons). In both cases, the long-time asymptotic states have a strong memory of the initial state and thus evade thermalization in its simplest form. The phenomena observed are reminiscent of the observations of the presence of highly non-thermal states in the quantum Ising model [13]. In a forthcoming paper [50] we will relate our findings to the intricate phase diagram of the BSM at equilibrium.

Interestingly, the initial confined core persists up to very long time, as witnessed by the entanglement entropy. We still need to understand if it ultimately disap-

pears or if it persists in the asymptotic regime, even for massless bosons. Unfortunately, our current numerical simulations cannot be extended beyond the time scales we have considered here. Such questions could hopefully be addressed using the next-generation of tensor-network methods (for recent proposal see [95] and references therein) and quantum simulators [46].

We thank Subhroneel Chakrabarti, Sanjukta Kundu, Marek M. Rams, Krzysztof Sacha, Piotr Sierant, Piotr Korcyl, Krzysztof Biedroń, Gert Aarts, Alessio Celi, Valentin Kasper, E. Miles Stoudenmire and Matthew Fishman for useful discussions. MPS algorithms have been implemented using ITensor library v2 (<https://itensor.org>). T. C. and J. Z. acknowledge support by PL-Grid Infrastructure and by National Science Centre (Poland) under QuantERA QT-FLAG project 2017/25/Z/ST2/03029. M.L. acknowledges support by the Spanish Ministry MINECO (National Plan 15 Grant: FISICATEAMO No. FIS2016-79508-P, SEVERO OCHOA No. SEV-2015-0522, FPI), European Social Fund, Fundació Cellex, Generalitat de Catalunya (AGAUR Grant No. 2017 SGR 1341 and CERCA/Program), ERC AdG OSYRIS and NOQIA, and the National Science Centre, Poland-Symfonia Grant No. 2016/20/W/ST4/00314. LT is supported by the MINECO RYC-2016-20594 fellowship and the MINECO PGC2018-095862-B-C22 grant.

* titas.chanda@uj.edu.pl

- [1] D. Fausti, R. I. Tobey, N. Dean, S. Kaiser, A. Dienst, M. C. Hoffmann, S. Pyon, T. Takayama, H. Takagi, and A. Cavalleri, *Science* **331**, 189 (2011).
- [2] D. A. Abanin and Z. Papić, *Annalen der Physik* **529**, 1700169 (2017).
- [3] F. Alet and N. Laflorencie, *Comptes Rendus Physique* **19**, 498 (2018).
- [4] M. Rigol, V. Dunjko, and M. Olshanii, *Nature* **452**, 854 (2008).
- [5] A. Polkovnikov, K. Sengupta, A. Silva, and M. Vengalattore, *Rev. Mod. Phys.* **83**, 863 (2011).
- [6] J. Eisert, M. Friesdorf, and C. Gogolin, *Nature Physics* **11**, 124 (2015).
- [7] L. D’Alessio, Y. Kafri, A. Polkovnikov, and M. Rigol, *Advances in Physics* **65**, 239 (2016).
- [8] E. Noether, *Nachrichten von der Gesellschaft der Wissenschaften zu Göttingen, Mathematisch-Physikalische Klasse* **1918**, 235 (1918).
- [9] O. A. Castro-Alvaredo, B. Doyon, and T. Yoshimura, *Phys. Rev. X* **6**, 041065 (2016).
- [10] B. Bertini, M. Collura, J. De Nardis, and M. Fagotti, *Phys. Rev. Lett.* **117**, 207201 (2016).
- [11] M. Brenes, M. Dalmonte, M. Heyl, and A. Scardicchio, *Phys. Rev. Lett.* **120**, 030601 (2018).
- [12] N. J. Robinson, A. J. A. James, and R. M. Konik, *Phys. Rev. B* **99**, 195108 (2019).
- [13] A. J. A. James, R. M. Konik, and N. J. Robinson, *Phys. Rev. Lett.* **122**, 130603 (2019).

[14] F. M. Surace, P. P. Mazza, G. Giudici, A. Lerose, A. Gambassi, and M. Dalmonte, [arXiv:1902.09551](https://arxiv.org/abs/1902.09551).

[15] J. Park, Y. Kuno, and I. Ichinose, *Phys. Rev. A* **100**, 013629 (2019).

[16] A. C. Cubero and N. J. Robinson, [arXiv:1908.00270](https://arxiv.org/abs/1908.00270).

[17] J. Schwinger, *Phys. Rev.* **82**, 664 (1951).

[18] J. Schwinger, *Phys. Rev.* **125**, 397 (1962).

[19] J. Schwinger, *Phys. Rev.* **128**, 2425 (1962).

[20] S. Coleman, *Annals of Physics* **101**, 239 (1976).

[21] C. Hamer, J. Kogut, D. Crewther, and M. Mazzolini, *Nuclear Physics B* **208**, 413 (1982).

[22] C. Adam, *Annals of Physics* **259**, 1 (1997).

[23] T. V. Zache, N. Mueller, J. T. Schneider, F. Jendrzejewski, J. Berges, and P. Hauke, *Phys. Rev. Lett.* **122**, 050403 (2019).

[24] T. M. R. Byrnes, P. Sriganesh, R. J. Bursill, and C. J. Hamer, *Phys. Rev. D* **66**, 013002 (2002).

[25] M. Bauls, K. Cichy, J. Cirac, and K. Jansen, *Journal of High Energy Physics* **2013**, 158 (2013).

[26] B. Buyens, J. Haegeman, K. Van Acoleyen, H. Verschelde, and F. Verstraete, *Phys. Rev. Lett.* **113**, 091601 (2014).

[27] S. Kühn, J. I. Cirac, and M.-C. Bañuls, *Phys. Rev. A* **90**, 042305 (2014).

[28] M. C. Bañuls, K. Cichy, J. I. Cirac, K. Jansen, and H. Saito, *Phys. Rev. D* **92**, 034519 (2015).

[29] B. Buyens, F. Verstraete, and K. Van Acoleyen, *Phys. Rev. D* **94**, 085018 (2016).

[30] T. Pichler, M. Dalmonte, E. Rico, P. Zoller, and S. Montangero, *Phys. Rev. X* **6**, 011023 (2016).

[31] M. C. Bañuls, K. Cichy, J. I. Cirac, K. Jansen, and S. Kühn, *Phys. Rev. Lett.* **118**, 071601 (2017).

[32] Y.-P. Huang, D. Banerjee, and M. Heyl, *Phys. Rev. Lett.* **122**, 250401 (2019).

[33] D. González-Cuadra, P. R. Grzybowski, A. Dauphin, and M. Lewenstein, *Phys. Rev. Lett.* **121**, 090402 (2018).

[34] D. González-Cuadra, A. Dauphin, P. R. Grzybowski, P. Wójcik, M. Lewenstein, and A. Bermudez, *Phys. Rev. B* **99**, 045139 (2019).

[35] D. González-Cuadra, A. Bermudez, P. R. Grzybowski, M. Lewenstein, and A. Dauphin, *Nature Communications* **10**, 2694 (2019).

[36] K. Kasamatsu, I. Ichinose, and T. Matsui, *Phys. Rev. Lett.* **111**, 115303 (2013).

[37] O. Dutta, L. Tagliacozzo, M. Lewenstein, and J. Zakrzewski, *Phys. Rev. A* **95**, 053608 (2017).

[38] D. González-Cuadra, E. Zohar, and J. I. Cirac, *New Journal of Physics* **19**, 063038 (2017).

[39] Y. Kuno, S. Sakane, K. Kasamatsu, I. Ichinose, and T. Matsui, *Phys. Rev. D* **95**, 094507 (2017).

[40] S. Nascimbène, Y.-A. Chen, M. Atala, M. Aidelsburger, S. Trotzky, B. Paredes, and I. Bloch, *Phys. Rev. Lett.* **108**, 205301 (2012).

[41] E. A. Martinez, C. A. Muschik, P. Schindler, D. Nigg, A. Erhard, M. Heyl, P. Hauke, M. Dalmonte, T. Monz, P. Zoller, and R. Blatt, *Nature* **534**, 516 (2016).

[42] H. Bernien, S. Schwartz, A. Keesling, H. Levine, A. Omran, H. Pichler, S. Choi, A. S. Zibrov, M. Endres, M. Greiner, V. Vuletić, and M. D. Lukin, *Nature* **551**, 579 (2017).

[43] N. Klco, E. F. Dumitrescu, A. J. McCaskey, T. D. Morris, R. C. Pooser, M. Sanz, E. Solano, P. Lougovski, and M. J. Savage, *Phys. Rev. A* **98**, 032331 (2018).

[44] F. Görg, K. Sandholzer, J. Minguzzi, R. Desbuquois, M. Messer, and T. Esslinger, *Nature Physics* (2019), [10.1038/s41567-019-0615-4](https://doi.org/10.1038/s41567-019-0615-4).

[45] C. Schweizer, F. Grusdt, M. Berngruber, L. Barbiero, E. Demler, N. Goldman, I. Bloch, and M. Aidelsburger, [arXiv:1901.07103](https://arxiv.org/abs/1901.07103).

[46] A. Mil, T. V. Zache, A. Hegde, A. Xia, R. P. Bhatt, M. K. Oberthaler, P. Hauke, J. Berges, and F. Jendrzejewski, [arXiv:1909.07641](https://arxiv.org/abs/1909.07641).

[47] J. Kogut and L. Susskind, *Phys. Rev. D* **11**, 395 (1975).

[48] M. Creutz, *Phys. Rev. D* **15**, 1128 (1977).

[49] M. Creutz, I. J. Muzinich, and T. N. Tudron, *Phys. Rev. D* **19**, 531 (1979).

[50] T. Chanda, J. Zakrzewski, M. Lewenstein, and L. Tagliacozzo, In preparation.

[51] U. Schollwöck, *Annals of Physics* **326**, 96 (2011).

[52] F. Verstraete and J. I. Cirac, [arXiv:cond-mat/0407066](https://arxiv.org/abs/cond-mat/0407066).

[53] R. Ors, *Annals of Physics* **349**, 117 (2014).

[54] J. C. Bridgeman and C. T. Chubb, *Journal of Physics A: Mathematical and Theoretical* **50**, 223001 (2017).

[55] S.-J. Ran, E. Tirrito, C. Peng, X. Chen, L. Tagliacozzo, G. Su, and M. Lewenstein, [arXiv:1708.09213](https://arxiv.org/abs/1708.09213).

[56] G. M. Crosswhite, A. C. Doherty, and G. Vidal, *Phys. Rev. B* **78**, 035116 (2008).

[57] P. Hauke, F. M. Cucchietti, A. Müller-Hermes, M.-C. Bañuls, J. I. Cirac, and M. Lewenstein, *New Journal of Physics* **12**, 113037 (2010).

[58] T. Koffel, M. Lewenstein, and L. Tagliacozzo, *Phys. Rev. Lett.* **109**, 267203 (2012).

[59] P. Hauke and L. Tagliacozzo, *Phys. Rev. Lett.* **111**, 207202 (2013).

[60] A. Milsted, J. Haegeman, and T. J. Osborne, *Phys. Rev. D* **88**, 085030 (2013).

[61] M. P. Zaletel, R. S. K. Mong, C. Karrasch, J. E. Moore, and F. Pollmann, *Phys. Rev. B* **91**, 165112 (2015).

[62] M. C. Bañuls, K. Cichy, J. I. Cirac, K. Jansen, and S. Kühn, *Phys. Rev. X* **7**, 041046 (2017).

[63] S. Paeckel, T. Khler, A. Swoboda, S. R. Manmana, U. Schollwöck, and C. Hubig, [arXiv:1901.05824](https://arxiv.org/abs/1901.05824).

[64] T. Sugihara, *Journal of High Energy Physics* **2005**, 022 (2005).

[65] L. Tagliacozzo and G. Vidal, *Phys. Rev. B* **83**, 115127 (2011).

[66] L. Tagliacozzo, A. Celi, and M. Lewenstein, *Phys. Rev. X* **4**, 041024 (2014).

[67] P. Silvi, E. Rico, T. Calarco, and S. Montangero, *New Journal of Physics* **16**, 103015 (2014).

[68] S. Kühn, E. Zohar, J. I. Cirac, and M. C. Bañuls, *Journal of High Energy Physics* **2015**, 130 (2015).

[69] J. Haegeman, K. Van Acoleyen, N. Schuch, J. I. Cirac, and F. Verstraete, *Phys. Rev. X* **5**, 011024 (2015).

[70] M. Kormos, M. Collura, G. Takcs, and P. Calabrese, *Nature Physics* **13**, 246 (2017).

[71] B. Craps, E. Lindgren, and A. Taliotis, *Journal of High Energy Physics* **2015**, 1 (2015).

[72] J. Abajo-Arrastia, E. da Silva, E. Lopez, J. Mas, and A. Serantes, *J. High Energ. Phys.* **2014**, 126 (2014).

[73] E. da Silva, E. Lopez, J. Mas, and A. Serantes, *J. High Energ. Phys.* **2015**, 38 (2015).

[74] E. da Silva, E. Lopez, J. Mas, and A. Serantes, *Journal of High Energy Physics* **2016**, 172 (2016).

[75] R. C. Myers, M. Rozali, and B. Way, *Journal of Physics A: Mathematical and Theoretical* **50**, 494002 (2017).

[76] C. J. Turner, A. A. Michailidis, D. A. Abanin, M. Serbyn, and Z. Papić, *Nature Physics* **14**, 745 (2018).

- [77] P. Sala, T. Rakovszky, R. Verresen, M. Knap, and F. Pollmann, [arXiv:1904.04266](https://arxiv.org/abs/1904.04266).
- [78] L. Vidmar and M. Rigol, *Journal of Statistical Mechanics: Theory and Experiment* **2016**, 064007 (2016).
- [79] M. E. Peskin and D. V. Schroeder, *An introduction to quantum field theory* (Addison-Wesley Pub. Co, Reading, Mass, 1995).
- [80] Supplementary material.
- [81] S. R. White, *Phys. Rev. Lett.* **69**, 2863 (1992).
- [82] S. R. White, *Phys. Rev. B* **48**, 10345 (1993).
- [83] U. Schollwöck, *Rev. Mod. Phys.* **77**, 259 (2005).
- [84] J. Haegeman, J. I. Cirac, T. J. Osborne, I. Pižorn, H. Verschelde, and F. Verstraete, *Phys. Rev. Lett.* **107**, 070601 (2011).
- [85] J. Haegeman, C. Lubich, I. Oseledets, B. Vandereycken, and F. Verstraete, *Phys. Rev. B* **94**, 165116 (2016).
- [86] P. Calabrese and J. Cardy, *Journal of Statistical Mechanics: Theory and Experiment* **2005**, P04010 (2005).
- [87] N. Schuch, F. Verstraete, and J. I. Cirac, *Phys. Rev. Lett.* **92**, 087904 (2004).
- [88] N. Schuch, F. Verstraete, and J. I. Cirac, *Phys. Rev. A* **70**, 042310 (2004).
- [89] W. Donnelly, *Phys. Rev. D* **85**, 085004 (2012).
- [90] D. Radicevic, [arXiv:1404.1391](https://arxiv.org/abs/1404.1391).
- [91] H. Casini, M. Huerta, and J. A. Rosabal, *Phys. Rev. D* **89**, 085012 (2014).
- [92] H. Casini, M. Huerta, J. M. Magan, and D. Pontello, [arXiv:1905.10487](https://arxiv.org/abs/1905.10487).
- [93] A. Lukin, M. Rispoli, R. Schittko, M. E. Tai, A. M. Kaufman, S. Choi, V. Khemani, J. Léonard, and M. Greiner, *Science* **364**, 256 (2019).
- [94] P. Sierant, K. Biedro, G. Morigi, and J. Zakrzewski, *SciPost Phys.* **7**, 8 (2019).
- [95] J. Surace, M. Piani, and L. Tagliacozzo, *Phys. Rev. B* **99**, 235115 (2019).

Supplementary material to “Confinement and lack of thermalization after quenches in bosonic Schwinger model”

Titas Chanda,^{1,*} Jakub Zakrzewski,^{1,2} Maciej Lewenstein,^{3,4} and Luca Tagliacozzo^{5,6}

¹*Instytut Fizyki im. Mariana Smoluchowskiego, Uniwersytet Jagielloński, Lojasiewicza 11, 30-348 Kraków, Poland*

²*Mark Kac Complex Systems Research Center, Uniwersytet Jagielloński, Kraków, Poland*

³*ICFO-Institut de Ciències Fotòniques, The Barcelona Institute of Science and Technology,*

Av. Carl Friedrich Gauss 3, 08860 Castelldefels (Barcelona), Spain

⁴*ICREA, Passeig Lluís Companys 23, 08010 Barcelona, Spain*

⁵*Department of Physics and SUPA, University of Strathclyde, Glasgow G4 0NG, UK*

⁶*Departament de Física Quàntica i Astrofísica and Institut de Ciències del Cosmos (ICCUB),*

Universitat de Barcelona, Martí i Franquès 1, 08028 Barcelona, Catalonia, Spain

We derive the Hamiltonian of the discretized version of the bosonic Schwinger model (BSM) and the Gauss law generators corresponding to the local $U(1)$ gauge symmetry. We also supplement the main text with the results for intermediate boson masses. Then we give an explicit demonstration of area-law of entanglement entropy in the confined domain. Finally, necessary information regarding numerical simulations using matrix product states (MPS) techniques performed in the main text are provided.

Derivation of the Hamiltonian

The Lagrangian density for the BSM [1] is given by

$$\mathcal{L} = -[D_\mu \phi]^* D^\mu \phi - m^2 |\phi|^2 - \frac{1}{4} F_{\mu\nu} F^{\mu\nu}, \quad (1)$$

where ϕ is the complex scalar field, $D_\mu = (\partial_\mu + iqA_\mu)$ is the covariant derivative with q and A_μ being the electronic charge and electromagnetic vector potential respectively, m is the mass of the particles, and $F_{\mu\nu}$ is the electromagnetic field tensor. Here, we use the metric convection $(-1, 1, 1, 1)$ or $(-1, 1)$ (in 1+1 dimensions). In 1+1 dimensions, after fixing the temporal gauge $A_t(x, t) = 0$, we get the quantum Hamiltonian as

$$\hat{H} = \int dx \left[\frac{1}{2} \hat{E}_x^2(x) + \hat{\Pi}^\dagger(x) \hat{\Pi}(x) + m^2 \hat{\phi}^\dagger(x) \hat{\phi}(x) + (\partial_x - iq\hat{A}_x(x)) \hat{\phi}^\dagger(x) (\partial_x + iq\hat{A}_x(x)) \hat{\phi}(x) \right], \quad (2)$$

where $\hat{E}_x(x)$, $\hat{\Pi}(x)$, and $\hat{\Pi}^\dagger(x)$ are the canonical conjugate operators corresponding to $\hat{A}_x(x)$, $\hat{\phi}(x)$, and $\hat{\phi}^\dagger(x)$ respectively, satisfying $[\hat{A}_x(x_1), \hat{E}_x(x_2)] = [\hat{\phi}(x_1), \hat{\Pi}(x_2)] = [\hat{\phi}^\dagger(x_1), \hat{\Pi}^\dagger(x_2)] = i\delta(x_1 - x_2)$. We can discretize this Hamiltonian on a 1D lattice having lattice-spacing a in a straightforward way such that the matter fields $\{\hat{\phi}_j, \hat{\phi}_j^\dagger, \hat{\Pi}_j, \hat{\Pi}_j^\dagger\}$ reside on lattice site j , while the gauge fields $\{\hat{A}_j, \hat{E}_j\}$ act on the bond between lattice points j and $j+1$. The Hamiltonian, thus discretized,

reads as

$$\hat{H} = \frac{a}{2} \sum_j \hat{E}_j^2 + \frac{1}{a} \sum_j \hat{\Pi}_j^\dagger \hat{\Pi}_j + \left(am^2 + \frac{2}{a} \right) \sum_j \hat{\phi}_j^\dagger \hat{\phi}_j - \frac{1}{a} \sum_j \left[\hat{\phi}_{j+1}^\dagger \exp(-iq\hat{A}_j) \hat{\phi}_j + \text{h.c.} \right], \quad (3)$$

where the operators have been rescaled to satisfy the commutation relations $[\hat{A}_j, \hat{E}_k] = [\hat{\phi}_j, \hat{\Pi}_k] = [\hat{\phi}_j^\dagger, \hat{\Pi}_k^\dagger] = i\delta_{jk}$. As the next few steps, we introduce bosonic operators \hat{a}_j and \hat{b}_j as

$$\begin{aligned} \hat{\phi}_j &= \frac{1}{\sqrt{2}} (\hat{a}_j + \hat{b}_j^\dagger), & \hat{\Pi}_j &= \frac{i}{\sqrt{2}} (\hat{a}_j^\dagger - \hat{b}_j), \\ \hat{\phi}_j^\dagger &= \frac{1}{\sqrt{2}} (\hat{a}_j^\dagger + \hat{b}_j), & \hat{\Pi}_j^\dagger &= \frac{i}{\sqrt{2}} (\hat{b}_j^\dagger - \hat{a}_j), \end{aligned} \quad (4)$$

rescale the gauge fields as $\hat{L}_j = \hat{E}_j/q$, $\hat{\theta}_j = q\hat{A}_j$, and multiply the Hamiltonian by $1/aq^2$ to make it dimensionless. The Hamiltonian now becomes

$$\begin{aligned} \hat{H} &= \sum_j \hat{L}_j^2 + ((m/q)^2 + 3x) \sum_j (\hat{a}_j^\dagger \hat{a}_j + \hat{b}_j \hat{b}_j^\dagger) \\ &+ ((m/q)^2 + x) \sum_j (\hat{a}_j^\dagger \hat{b}_j^\dagger + \hat{a}_j \hat{b}_j) \\ &- x \sum_j \left[(\hat{a}_{j+1}^\dagger + \hat{b}_{j+1}^\dagger) \hat{U}_j (\hat{a}_j + \hat{b}_j^\dagger) + \text{h.c.} \right], \end{aligned} \quad (5)$$

where $\hat{U}_j = \exp(-i\hat{\theta}_j)$ and $\hat{U}_j^\dagger = \exp(i\hat{\theta}_j)$ are the ladder operators satisfying $[\hat{L}_j, \hat{U}_j] = -\hat{U}_j$ and $[\hat{L}_j, \hat{U}_j^\dagger] = \hat{U}_j^\dagger$ respectively, and $x = 1/a^2q^2$. To further simplify the Hamiltonian, we employ a local Bogoliubov transformation as

$$\begin{aligned} \hat{a}_j &\rightarrow \cosh(\theta_j) \hat{a}_j + \sinh(\theta_j) \hat{b}_j^\dagger, \\ \hat{b}_j &\rightarrow \cosh(\theta_j) \hat{b}_j + \sinh(\theta_j) \hat{a}_j^\dagger, \end{aligned} \quad (6)$$

where $\theta_j = -\frac{1}{2} \tanh^{-1} \left[\frac{(m/q)^2 + x}{(m/q)^2 + 3x} \right]$ for all j , such that our final Hamiltonian is given as

$$\hat{H} = \sum_j \hat{L}_j^2 + 2 \left(x \left((m/q)^2 + 2x \right) \right)^{1/2} \sum_j (\hat{a}_j^\dagger \hat{a}_j + \hat{b}_j^\dagger \hat{b}_j) - \frac{x^{3/2}}{\left((m/q)^2 + 2x \right)^{1/2}} \sum_j \left[(\hat{a}_{j+1}^\dagger + \hat{b}_{j+1}) \hat{U}_j (\hat{a}_j + \hat{b}_j^\dagger) + \text{h.c.} \right]. \quad (7)$$

We refer the bosons ‘ a ’ and ‘ b ’ as particles and antiparticles respectively.

Local gauge invariance and Gauss law generators

It can be straightforwardly verified that the Hamiltonian in Eq. (7) is invariant under local $U(1)$ gauge transformations:

$$\hat{a}_j \rightarrow e^{i\alpha_j} \hat{a}_j, \quad \hat{b}_j \rightarrow e^{-i\alpha_j} \hat{b}_j, \quad (8)$$

$$\hat{U}_j \rightarrow e^{-i\alpha_j} \hat{U}_j e^{i\alpha_{j+1}}. \quad (9)$$

Corresponding Gauss law generators can be obtained from the Euler-Lagrange equation of the field A_t , i.e.,

$$\left[\partial_\mu \left[\frac{\partial \mathcal{L}}{\partial (\partial_\mu A_t)} \right] - \frac{\partial \mathcal{L}}{\partial A_t} \right]_{A_t \rightarrow 0} = 0, \\ \Rightarrow \partial_x E_x(x) = iq (\phi^*(x) \Pi^*(x) - \phi(x) \Pi(x)), \quad (10)$$

which, after quantization with normal ordering and discretization similar to the Hamiltonian, gives us the Gauss law generators as

$$\hat{G}_j = \hat{L}_j - \hat{L}_{j-1} - \underbrace{\left(\hat{a}_j^\dagger \hat{a}_j - \hat{b}_j^\dagger \hat{b}_j \right)}_{\hat{Q}_j}, \quad (11)$$

where the dynamical charge, $\hat{Q}_j = \hat{a}_j^\dagger \hat{a}_j - \hat{b}_j^\dagger \hat{b}_j$, is basically the difference between the particle-antiparticle number. In the absence of any background static charges, the physical sector is spanned by the states satisfying $\hat{G}_j = 0$ for all values of j . Using this constraint imposed by the Gauss law, we can integrate-out the gauge-fields for a chain with open-boundary condition using the following transformation,

$$\left[\prod_{l < j} \hat{U}_l \right] \hat{a}_j \rightarrow \hat{a}_j, \quad \left[\prod_{l < j} \hat{U}_l^\dagger \right] \hat{b}_j \rightarrow \hat{b}_j, \quad \hat{L}_j = \sum_{l \leq j} \hat{Q}_l, \quad (12)$$

where the background static field at the left of the chain has been considered to be zero.

Dynamics for intermediate boson masses

Fig. 1 shows the dynamics of both the gauge sector (\hat{L}_j) and the charge sector (\hat{Q}_j) for boson masses $m/q = 0.25, 0.5$, and 1 for $R = 5$. Clearly, as the mass increases the confining behavior of the dynamics becomes stronger, as the coherent oscillation of the confined core

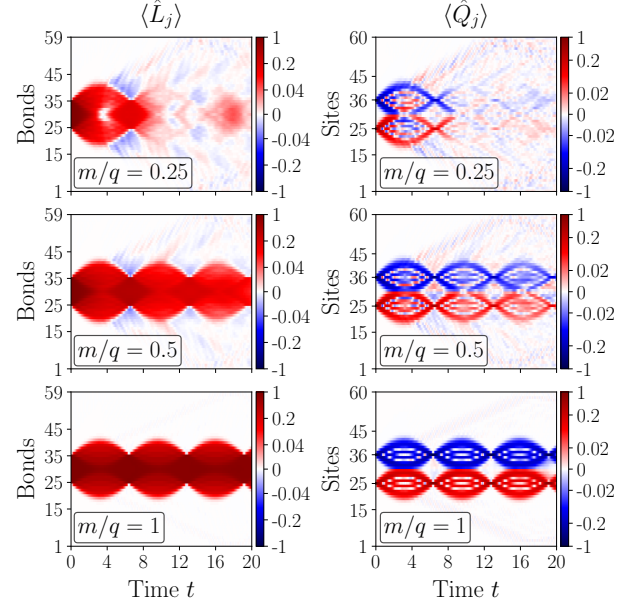


FIG. 1. (Color online.) Dynamics of electric field $\langle \hat{L}_j \rangle$ (left column) and dynamical charge $\langle \hat{Q}_j \rangle$ (right column) for $m/q = 0.25$ (top row), 0.5 (middle row), and 1 (bottom row) and $R = 5$.

lasts longer. For example, there is no string-inversion for $m/q = 0.25$ before $t = 8$, and the string does not break in the bulk for $m/q = 0.5$. On the other hand, we already reach the heavy boson limit with $m/q = 1$.

The classical (\mathcal{S}^C) and the distillable (\mathcal{S}^Q) parts of entanglement entropy shows similar features for these intermediate masses (Fig. 2). The distinction between the deconfined domain and the confined core, as perceived from the classical part, is becomes much more pronounced for $m/q = 0.25$ and 0.5 than the massless scenario depicted in the main text.

Area-law of entanglement entropy in the confined domain

We follow the entanglement dynamics for system sizes $N = 60, 80$, and 100 with $R = N/10$ so that the initial string length increases with system size. The average entropy in the confined domain, i.e.,

$$\mathcal{S}^{Av} = \frac{1}{2R+1} \sum_{j=N/2-R}^{N/2+R} \mathcal{S}_j \quad (13)$$

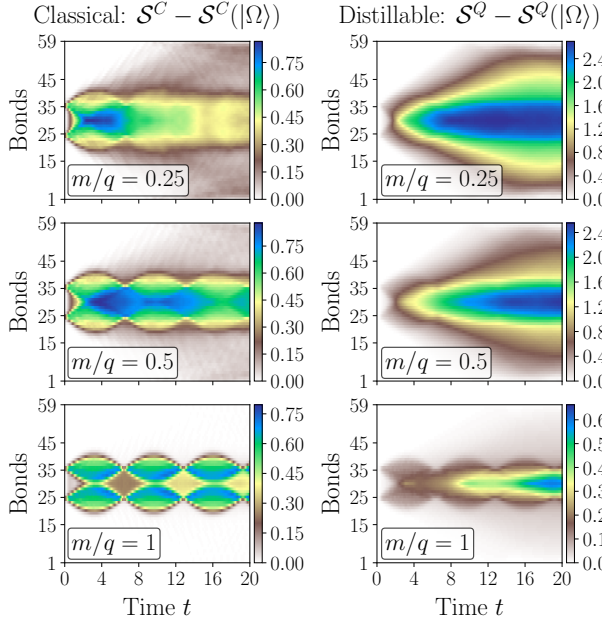


FIG. 2. (Color online.) Time-evolution the classical part S^C of entanglement entropy (left column) and the distillable entanglement entropy S^Q (right column) for $m/q = 2.5$ (top row), 0.5 (middle row), and 1 (bottom row) and $R = 5$.

follows area-law of entanglement throughout the dynamics as it remains (almost) invariant with system size as shown in Fig. 3.

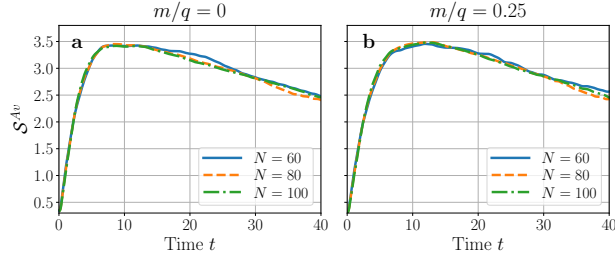


FIG. 3. (Color online.) Evolution of average entropy in the confined domain for different system sizes. Here we consider $R = N/10$ so that it grows proportional to the system size.

Details about tensor network simulation

We use matrix product states (MPS) [2, 3] ansatz with open boundary condition to simulate states of the system, where we integrate-out the gauge fields using the Gauss law. Due to this tracing-out of the gauge fields, we do not need to use gauge-invariant tensor network [4–7] for our calculations. However, we use global $U(1)$ symmetry [8, 9] corresponding to the conservation of total dy-

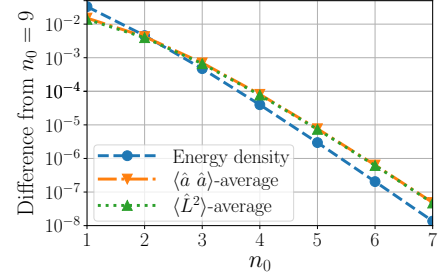


FIG. 4. (Color online.) Dependence of physical quantities on the boson number cutoff n_0 in the ground state of the system for $m/q = 0$. Here we plot the difference between the values of different observables computed for different values of n_0 from $n_0 = 9$. Clearly, for $n_0 = 5$ the error due to the truncated bosonic Hilbert space falls below 10^{-5} .

nanical charge, $\sum_j \hat{Q}_j$, and obviously we work only in the $\sum_j \langle \hat{Q}_j \rangle = 0$ sector. The maximum number bosons (n_0) per site for each species has been truncated to 5, resulting in a physical dimension of 36 on each site. This truncation is justified as the densities of the bosons never cross ~ 1.5 throughout our simulation. We confirm this by checking the convergence of several observables with respect to n_0 in the ground-state of the model in Fig. 4, where we show that for $m/q = 0$ the errors due to this truncation is below 10^{-5} for $n_0 = 5$. One important thing to mention here that it is also possible to separate-out two types of bosons to odd and even lattice-sites respectively maintaining global $U(1)$ symmetry, such that physical dimension on each site only grows linearly with n_0 . This will definitely increase efficiency of the simulation for a given MPS bond dimension. However, as two types of bosons sitting on a same site are *strongly* correlated, such method of separating them out using truncated bonds will incur much more errors, especially in the time-evolution, and needs much larger bond dimension to get converged results.

To find the ground state of the system, first we use two-site density matrix renormalization group (DMRG) [10–12] upto a maximum bond dimension $D_{max} \leq 100$, so that largest SVD truncation error with D_{max} remains below 10^{-12} . After that we switch to one-site variational optimization (“one-site DMRG”) [2, 13] for more stringent convergence within the MPS manifold given by D_{max} .

Time-evolution using MPS ansatz (tensor network in general) is always tricky, error-prone, and therefore must be dealt with caution, as entanglement entropy grows ballistically in the dynamics, which, in turn, demands larger and larger MPS bond dimension. Recently, to tackle such issues, the time-dependent variational principle (TDVP) algorithm [14–16] has been developed, which has been argued to be much less error-prone than earlier methods, e.g., time evolving block decimation (TEBD),

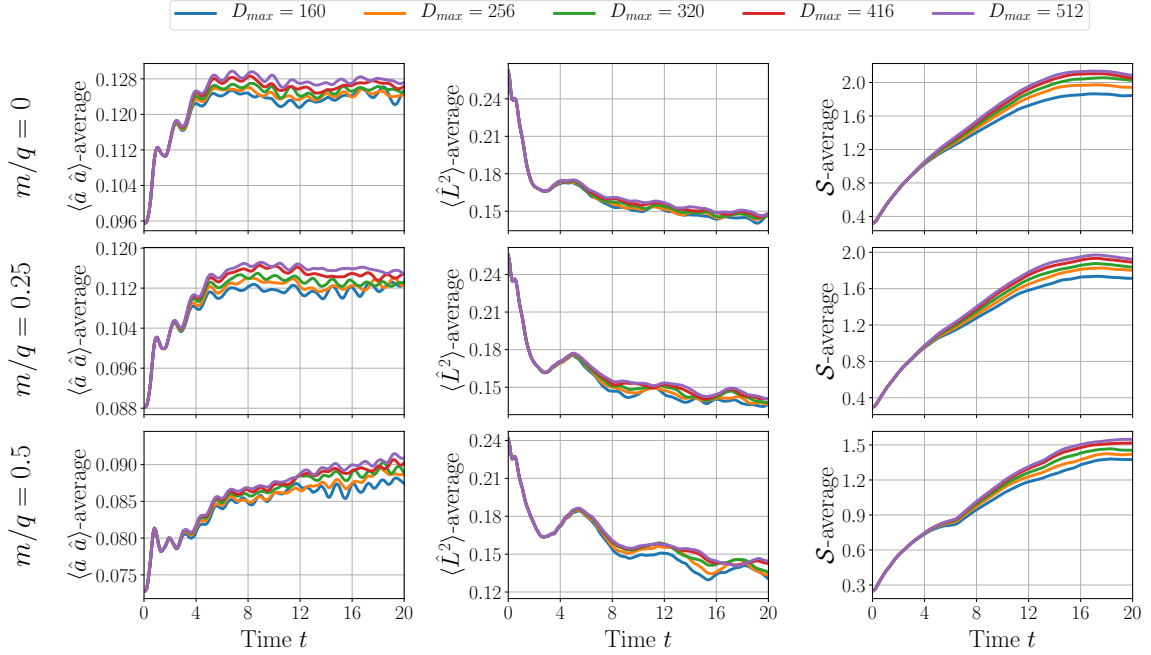


FIG. 5. (Color online.) Time-evolution of different physical observables using hybrid TDVP for different bond-dimensions. We plot the averages of $\langle \hat{a}^\dagger \hat{a} \rangle$ (left column), $\langle \hat{L}^2 \rangle$ (middle column), and the entanglement entropy \mathcal{S} (right column) as function of time upto $t = 20$ for $m/q = 0, 0.25$, and 0.5 .

within a given bond dimension [17]. Here we employ “hybrid” TDVP with step-size $\delta t = 0.01$, where we first use two-site version of TDVP to dynamically grow the bond dimension upto $D_{max} = 512$. When the bond dimension in the bulk of the MPS is saturated to $D_{max} = 512$, we switch to the one-site version to avoid any error due to SVD truncation. This hybrid method of time-evolution using TDVP has been argued to incur much less error than other known methods [17, 18]. It is noteworthy to mention here that since we use properly converged Lanczos exponentiation [19] in TDVP simulations, different step-sizes do not alter the results. To be assured of the trustworthiness of our simulations, we also perform TDVP simulations for $D_{max} = 160, 256, 320$, and 416 and check the convergence of different observables with respect to different D_{max} (see Fig. 5 for the case of $N = 60$ and $R = 5$). Clearly, upto $t \approx 4$, all the graphs, including $D_{max} = 160$ simulations, are converged, even when tallied in the light of entanglement entropy \mathcal{S} , which is believed to behave much worse in truncated bond dimensions. On the other hand, $D_{max} = 416$ data remain satisfactorily close to $D_{max} = 512$ curves throughout the time window, showing the reliability of our simulation with the bond dimension $D_{max} = 512$. For heavier masses, e.g., $m/q = 1.2$ (not shown in the figure), all the quantities are converged for every bond dimension considered here.

* titas.chanda@uj.edu.pl

- [1] M. E. Peskin and D. V. Schroeder, *An introduction to quantum field theory* (Addison-Wesley Pub. Co, Reading, Mass, 1995).
- [2] U. Schollwck, *Annals of Physics* **326**, 96 (2011).
- [3] R. Ors, *Annals of Physics* **349**, 117 (2014).
- [4] L. Tagliacozzo, A. Celi, and M. Lewenstein, *Phys. Rev. X* **4**, 041024 (2014).
- [5] B. Buyens, J. Haegeman, K. Van Acoleyen, H. Verschelde, and F. Verstraete, *Phys. Rev. Lett.* **113**, 091601 (2014).
- [6] P. Silvi, E. Rico, T. Calarco, and S. Montangero, *New Journal of Physics* **16**, 103015 (2014).
- [7] I. Kull, A. Molnar, E. Zohar, and J. I. Cirac, *Annals of Physics* **386**, 199 (2017).
- [8] S. Singh, R. N. C. Pfeifer, and G. Vidal, *Phys. Rev. A* **82**, 050301 (2010).
- [9] S. Singh, R. N. C. Pfeifer, and G. Vidal, *Phys. Rev. B* **83**, 115125 (2011).
- [10] S. R. White, *Phys. Rev. Lett.* **69**, 2863 (1992).
- [11] S. R. White, *Phys. Rev. B* **48**, 10345 (1993).
- [12] U. Schollwöck, *Rev. Mod. Phys.* **77**, 259 (2005).
- [13] S. R. White, *Phys. Rev. B* **72**, 180403 (2005).
- [14] J. Haegeman, J. I. Cirac, T. J. Osborne, I. Pižorn, H. Verschelde, and F. Verstraete, *Phys. Rev. Lett.* **107**, 070601 (2011).
- [15] T. Koffel, M. Lewenstein, and L. Tagliacozzo, *Phys. Rev. Lett.* **109**, 267203 (2012).
- [16] J. Haegeman, C. Lubich, I. Oseledets, B. Vandereycken,

and F. Verstraete, *Phys. Rev. B* **94**, 165116 (2016).

[17] S. Paeckel, T. Khler, A. Swoboda, S. R. Manmana, U. Schollwck, and C. Hubig, [arXiv:1901.05824](https://arxiv.org/abs/1901.05824).

[18] S. Goto and I. Danshita, *Phys. Rev. B* **99**, 054307 (2019).

[19] M. Hochbruck and C. Lubich, *SIAM Journal on Numerical Analysis* **34**, 1911 (1997).